Simultaneous Spatial and Spectral Selectivity by Spatiotemporal Encoding

Jean-Nicolas Dumez, Rita Schmidt, and Lucio Frydman*

Purpose: To introduce a method that provides simultaneous spatial and spectral selectivity, whose implementation is less demanding than—and quality comparable to—conventional 2D spectral-spatial counterparts.
Theory: Spatiotemporal encoding concepts lead to a spatially selective, chemical-shift-dependent echo, with simultaneous dephasing of all other off-resonant species. The approach only requires applying a pair of suitable radiofrequency-swept pulses, and allows arbitrary shaping of the spatial profiles.
Methods: Based on arguments derived for chirp pulses operating in the sequential-sweep approximation, quadratic-phase SLR excitation and refocusing waveforms were designed and used to collect 2D slice- and shift-selective images on a 7 T microimaging system (phantoms). The same strategy was used to obtain multi-slice echo-planar and spin-echo images of breast on human volunteers in a 3 T scanner.
Results: The method managed to deliver excellent shift-selective multi-slice images in phantoms and human volunteers. Simultaneous water and fat images were also collected in a single, interleaved acquisition mode on both platforms, using straightforward sequence and reconstruction modifications of the basic scheme.
Conclusion: A new way to achieve chemical shift selectivity with high quality spatial profiling is achieved, without the usual requirements for playing out fast oscillating gradients in conjunction with carefully timed radiofrequency pulses. **Magn Reson Med 71:746–755, 2014. © 2013 Wiley Periodicals, Inc.**

Key words: spectral-spatial pulses; frequency-swept pulses; spatiotemporal encoding; spin-echo imaging; fat suppression; breast EPI

The ability to address a single resonance in a spatially restricted region is often needed in magnetic resonance imaging and spectroscopy [MRI, MRS, (1,2)]. Pulses that are simultaneously spatially and spectrally selective (3), so called SPSP pulses, have proven useful to achieve such task. SPSP pulses are typically used for selectively exciting the water resonance in multi-slice 2D imaging studies of fat-containing tissues like brain, liver, or breast. This is an important prerequisite of sequences that, like echo-planar imaging (EPI), are prone to chemical shift artifacts; water selectivity is also an integral component of musculoskeletal studies. In this respect, SPSP approaches have proven more robust than alternative fat saturation techniques (4). More recently, 2D spectral-spatial pulses have also been exploited for fast spectroscopic imaging of hyperpolarized metabolites (5). Most implementations of SPSP pulses rely on the concept of a joint k/*t*-space excitation (6), and on the application of suitably shaped radiofrequency (RF) pulses played in conjunction with oscillating gradients.

Frequency-swept pulses in general, and linearly-swept "chirp" pulses in particular, are a different kind of RF manipulation that also plays key roles in MRS and MRI (7,8). Depending on their resonance offsets, spins will precess in these manipulations for effectively different time periods. This will result in a net dephasing, which can be suppressed using various strategies (8–11). It has also been recognized that frequency-swept pulses carry the key for performing a so-called spatiotemporal encoding (SPEN) of the spins' evolution. This process can be exploited to collect arbitrarily high multidimensional images, spectra, or spectroscopic images within a single scan (12). In MRI, SPEN thereby provides an alternative to EPI (13–16); in 2D MRS (17–19) it provides a general approach, for which no other "ultrafast" alternatives exist.

In this study, we explore the usefulness of SPEN concepts as means to add spectral selectivity to a spatially sculpted excitation. It is shown that this can be simply achieved by a combination of two frequency sweeps, of the kind normally employed to encode chemical-shift information in "ultrafast" 2D MRS. By contrast to classic 2D SPSP pulses, the ensuing approach does not require fast oscillating gradients; its spatial selectivity is not limited either by demands placed by the spectral-domain excitation profile. In the following paragraph, the principles of this new form of spectral-spatial selectivity are derived, details of its implementation are given, and its use is illustrated with phantom experiments at 7 T and with human imaging scans at 3 T. These experiments exemplify fat suppression with simultaneous spatial selection and the concurrent acquisition of slice-selective images for multiple chemical species.

THEORY

Spatiotemporal Encoding as a Selective Spectral-Spatial Excitation Approach

Although the principles of ultrafast 2D MRS spectroscopy have been described in detail (12,18,19), it is convenient to revisit their use for the specific purpose of

Department of Chemical Physics, Weizmann Institute of Science, Rehovot 76100, Israel.

Grant sponsors: Marie Curie Action ITN METAFLUX (project 264780), DIP network (project 710907, Ministry of Education and Research, Germany), ERC advanced grant (project 246754), Kamin-Yeda Grant, Helen and Kimmel Award for Innovative Investigation, Perlman Family Foundation.

*Correspondence to: Lucio Frydman, Department of Chemical Physics, Weizmann Institute of Science, Rehovot 76100, Israel. E-mail: lucio.frydman@weizmann.ac.il

Received 12 December 2012; revised 5 February 2013; accepted 9 February 2013.
DOI 10.1002/mrm.24718
Published online 14 March 2013 in Wiley Online Library (wileyonlinelibrary.com).

this study, addressing joint SPSP selectivity. SPEN departs from traditional schemes in that instead of triggering the chemical shift evolution homogenously, it allows various chemical sites to accrue their spin evolution in a spatially heterogeneous fashion. Several alternatives have been proposed for achieving this (20,21); for concreteness we consider the application of a chirp pulse lasting a time T_e, sweeping a range of offsets ΔO while spins of a given chemical shift Ω—as measured vis-à-vis a carrier offset centered at Ω_{ref}—are under the action of a gradient G_e. Assuming that the usual principles of frequency sweeps are fulfilled ($\Delta O T_e >> 1$, negligible relaxation, small tip angle approximation), different positions will be endowed with a quadratic phase given by (11,12,22):

$$\phi_{exc}^{chirp}(z) = \gamma G_e \frac{T_e}{2}(z - z_c) - \frac{1}{2}\Delta O T_e \left(\frac{z - z_c}{L}\right)^2 - T_e \Omega \left(\frac{z - z_c}{L}\right) + \phi_{exc}^{0'} \quad [1]$$

where $L = \frac{\Delta O}{\gamma G_e}$ is the length of the excited region and z_c the slice center for the on-resonance species. The last term in Eq. [1] is a constant hereon disregarded. The final aim of SPEN MRS is to impart an evolution phase that is proportional to both the spins' chemical shift and to their spatial coordinate: $\phi_{evol}(z) = C\Omega(z - z_c)$, where C is a spatiotemporal constant under the experimentalist's control. Although the quadratic phase in Eq. [1] complicates this goal, this term can be removed by applying a suitable, additional frequency-swept pulse. This second sweep can take many different forms (20,21); for concreteness, we center on a 180° pulse, sweeping the same region addressed by the excitation but in half the time; i.e., $T_r = T_e/2$. With this configuration, the first and second frequency-swept pulses can be used as the slice-selective excitation and refocusing pulses of a spin-echo imaging experiment, respectively. When gradients of equal signs and equal senses of sweep are used for excitation and refocusing, i.e., $G_e = G_r$, a full and simultaneous rephasing of all terms is obtained regardless of chemical shifts; this option has been used for spin-echo imaging with several families of frequency-swept pulses (23–25). Alternatively, if as shown in Figure 1 the sweeps are kept equally signed but a bipolar gradient with $G_r = -G_e$ is applied, the quadratic term in Eq. [1] vanishes but a site-dependent linear chemical shift term of the kind being sought remains (25–28). Figure 1b illustrates the spatial characteristics that will then arise for two sites with different chemical shifts. The spatial characteristics of the excited slice will be given by the initial O_i and final O_f frequencies, as well as by the profile of the $B_1^+(t)$ excitation RF pulse. As for the chemical shift effects, this pulse combination will lead to a phase

$$\phi_{CS}(z) = 2T_e\ \Omega\ \frac{z - z_c}{L} \quad [2]$$

Given the z-linearity in this equation, a generic Ω will lead to a null overall signal arising from the chosen slice. A suitable post-inversion k_{cs}, however, can bring any particular chemical site into a constructive superposition

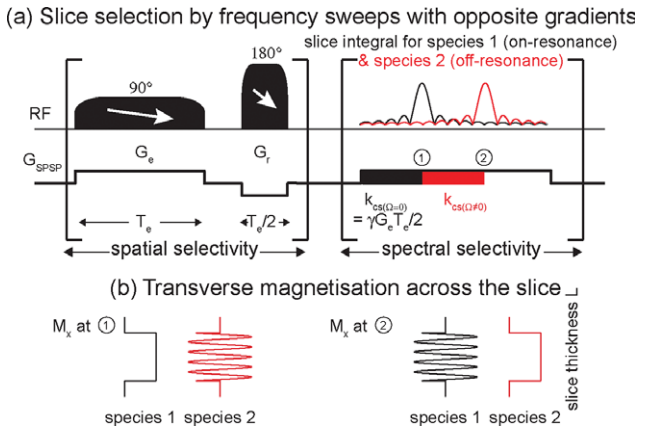

FIG. 1. Mechanism for simultaneous chemical shift and slice selection in an imaging experiment, based on applying a pair of frequency-swept pulses with opposite gradients. Following the spatial excitation, a rephasing gradient of area $k_{CS(\Omega=0)} = \frac{\gamma G_e T_e}{2}$ (black) leads to rephasing of the on-resonance species across the slice; the contribution of off-resonance species to signal is cancelled by a through-slice dephasing. An additional gradient lobe k_{CS} (red) can be used to put an off-resonance species back in phase. The RF amplitude was assumed constant leading to a square-like pattern; amplitude modulation of the first pulse would result in other profiles.

throughout the slice, leading to a site-specific observable signal. This is the principle used by SPEN for the ultrafast acquisition of indirect-domain spectra (17); the important point to highlight in the present context is the fact that an appropriate choice of the pulse duration T_e enables this refocusing to visualize one chosen species in the targeted slice, while dephasing the signals of all remaining off-resonance species excited in the region L.

The site-specific response arising from this scheme, assuming for simplicity a uniform spin density ρ across the excited slice L, is given by:

$$I(\Omega) \propto \frac{1}{L}\int_{-(L-\delta)/2}^{(L-\delta)/2} \rho(z')\exp\left(2i\Omega T_e \frac{z'}{L}\right)dz' \underset{\rho\approx 1}{\approx} \frac{\sin\left[\Omega T_e\left(1 - \frac{\delta}{L}\right)\right]}{\Omega T_e} \quad [3]$$

where $\delta = \frac{2\Omega}{\gamma G_e}$ is a change in slice thickness brought about by the targeted chemical shift offset. For an off-resonance species, the chemical shift will introduce opposite-signed displacements during the excitation and refocusing processes. Only the fraction of the slice that undergoes both pulses contributes to the signal; the remaining spins excited/inverted in the slice will stay longitudinal or be suppressed by crusher gradients. For reasonable gradient and shift values, this loss is expected to be minor. For multi-slice acquisitions, the existence of this slice displacement does not influence the inter-slice spacing that can be achieved; in particular, contiguous slices can be used and the full slice width ($\delta = 0$) can always be achieved for the on-resonance species.

It follows from Eq. [3] that the SPEN-based pulse pair introduces a sinc-like selectivity vis-à-vis offset. For a given pair of sites located a (known) $\Delta\Omega$ shift separation

apart, a zero of this function can be set by choosing a sweep of duration

$$T_e = p\frac{\pi}{\Delta\Omega}\left(1-\frac{2\Delta\Omega}{\gamma G_e L}\right)^{-1} \quad [4]$$

thus obtaining optimal suppression. p in this equation is an integer whose value can be adjusted to accommodate a maximum RF amplitude that is within hardware limitations for the desired bandwidth. As expected from Fourier principles, Eq. [4] implies that the minimum separation between the selected and suppressed resonances will be inversely proportional to the duration used for the chirp-driven SPEN encoding (for $p = 1$). By contrast to conventional 2D SPSP pulses, this will also be the time-scale available for achieving selectivity along the spatial dimension. This time is about an order of magnitude longer than what is usually available in the 2D SPSP pulses, boding well in terms of slice selectivity and spatial shaping.

METHODS

Pulse Design Considerations

Whereas the various arguments above were derived in terms of frequency-sweep concepts, the actual RF pulses used in this work were designed in their majority using the SLR algorithm (29). This was found important for achieving optimal spatial selectivity and signal intensity. Various modifications to the original SLR algorithm have been suggested to design nonlinear-phase pulses of the kind demanded by SPEN-based sequences (30–32). One such possibility consists of applying the desired nonlinear phase to the SLR B-polynomial in the frequency domain, prior to the inverse SLR transformation (30). Using this approach, a pulse can be designed that excites selectively the targeted band, with a phase:

$$\phi_{exc}^{SLR}(z) = \gamma G_e \frac{T_e}{2}(z-z_c) - \frac{1}{2}\Delta O T_e' \left(\frac{z-z_c}{L}\right)^2 + \phi_{exc}^0 \quad [5]$$

This is akin to Eq. [1] for an on-resonance species (i.e., with $\Omega = 0$), and its main difference involves a modification of the quadratic-phase coefficient given by a controllable T_e'. T_e' can be identified as the duration of the frequency sweep, which will actually end up being slightly shorter than total duration of the actual pulse, T_e. This difference between the sweeping duration and the pulse time is invested by the SLR algorithm into improving the high-frequency features associated with the desired spatial excitation profile; in particular, for sharpening the transition regions of the slice-selective manipulations. Figure 2 shows examples of the resulting quadratic-phase SLR excitation pulses. Qualitative mechanistic features based on chirp-pulse arguments can be appreciated from the plots in panel (a), including the fact that an approximately linear frequency sweep occupies a duration $T_e' < T_e$; Figure 2b and c also provides numerical examples of the spatial and spectral selectivity profiles that can be obtained with this SLR approach. When dealing with off-resonance species, a chemical-shift dependent linear phase term will also arise. This is

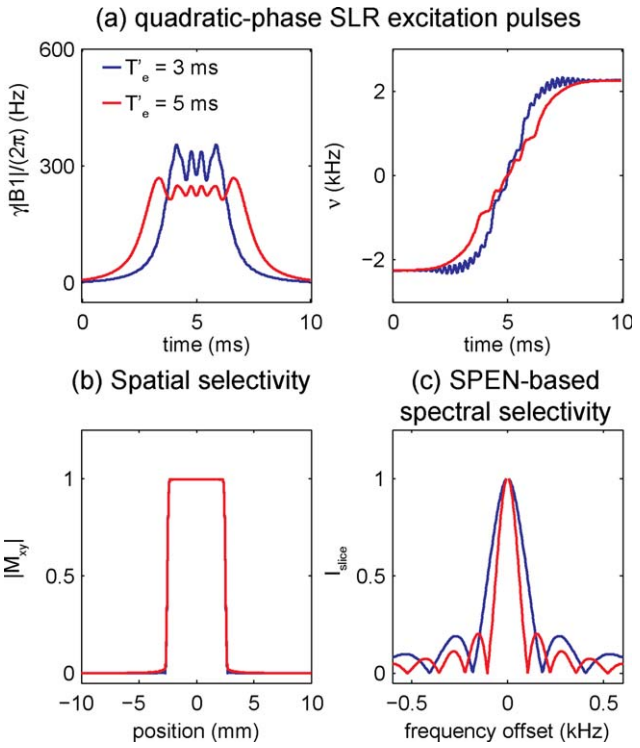

FIG. 2. **a**: Amplitude and frequency modulations calculated for representative SLR excitation pulses of the kind used in this study, illustrated for swept chirps of identical nominal duration $T_e = 10$ ms and bandwidth $\Delta O = 4.5$ kHz. As described in the text, SLR pulses are then ascribed frequency sweeps of variable durations; e.g., $T_e' = 3$ ms (blue) or 5 ms (red). **b**,**c**: Resulting spatial, spectral profiles arising upon implementing Bloch simulations based on the quadratic-phase SLR pulses, for the two chosen parameters. [Color figure can be viewed in the online issue, which is available at wileyonlinelibrary.com.]

naturally relevant for the SPEN process, and demands adding into Eq. [5] an additional chemical-shift winding term that is also T_e'-dependent:

$$\phi_{CS}^{SLR} = 2T_e'\Omega\frac{z-z_c}{L}. \quad [6]$$

Refocusing pulses were also here designed with the SLR algorithm; the condition required to remove the quadratic-phase imparted by the excitation will still be $T_r' = T_e'/2$—provided that both pulses have the same bandwidth.

The general properties of frequency sweeps remain relevant for quadratic-phase SLR pulses (30). For a given duration and bandwidth, these sweeps will result in lowered maximum RF amplitudes, allowing one to cover wider bands without exceeding maximum RF limitations. This, however, is achieved at the cost of an increased overall power deposition. Although specific parameter relations have to our knowledge not yet been fully derived for quadratic-phase SLR pulses, excellent selectivity could be obtained with simple choices of design parameters for the linear-phase filters. In this specific study, a least-squares finite-impulse-response filter with a time step of 8 μs, a fractional transition width of 0.2, and equal weights for the passband and stopband characteristics were successfully employed.

Phantom Experiments

The performance of the SPEN-based SPSP selectivity was assessed on phantom experiments carried out at 7 T using a Millipede® probe on a VNMRS 300/89 vertical-bore microimaging system (Varian Associates, Palo Alto, CA). The phantom consisted of two tubes of 11 mm inner diameter each filled respectively with water and with oil and placed side-by-side. 2D spin-echo images were obtained after applying the SPEN strategy in Figure 1, with the SPEN spatial selectivity applied along either the slice-selective or the readout dimensions. When the SPEN-based pulses were used in the readout dimension, an additional (conventional) refocusing pulse was inserted between the second frequency-swept pulse and data acquisition for slice selection purposes. Phantom experiments were also performed at 3 T on a Siemens Tim Trio clinical system (Siemens Healthcare, Erlangen, Germany) using a four-channel head coil. This phantom consisted of four water-containing spheres immersed in oil. 2D spin-echo images were obtained after a slice-selective SPEN-based pulse pair and compared against results obtained with a scanner-supplied SPAIR fat-suppressing sequence (33), and against a custom-written extended two-point Dixon approach (34,35).

Human Imaging Experiments

The SPEN SPSP selectivity performance was also assayed by breast imaging studies on human volunteers. These experiments were performed at 3 T on the Siemens Tim Trio clinical system using a four-channel breast coil, according to procedures approved by the Internal Review Board of the Wolfson Medical Center (Holon, Israel) and after obtaining suitable informed written consents of the volunteers. The SPEN-based excitation mode in Figure 1 was implemented in three different imaging strategies. (i) Water-only 2D multi-shot spin-echo images were collected after a slice-selective SPEN-based pulse pair, and compared against results arising from a scanner-supplied sequence involving fat suppression. (ii) 2D single-shot spin-echo EPI images using a SPEN-based pulse pair were compared against reference images obtained using a Siemens-supplied 2D SPSP pulse for selective water excitation. (iii) Concurrent water and fat images were collected following a pair of SPEN-based pulses, in a readout-interleaved fashion. This interleaving included the addition of suitable k_{cs} gradient lobes, effectively alternating back-and-forth among positions "1" and "2" in the spectral echoes of the water and fat resonances (Fig. 1). These gradient

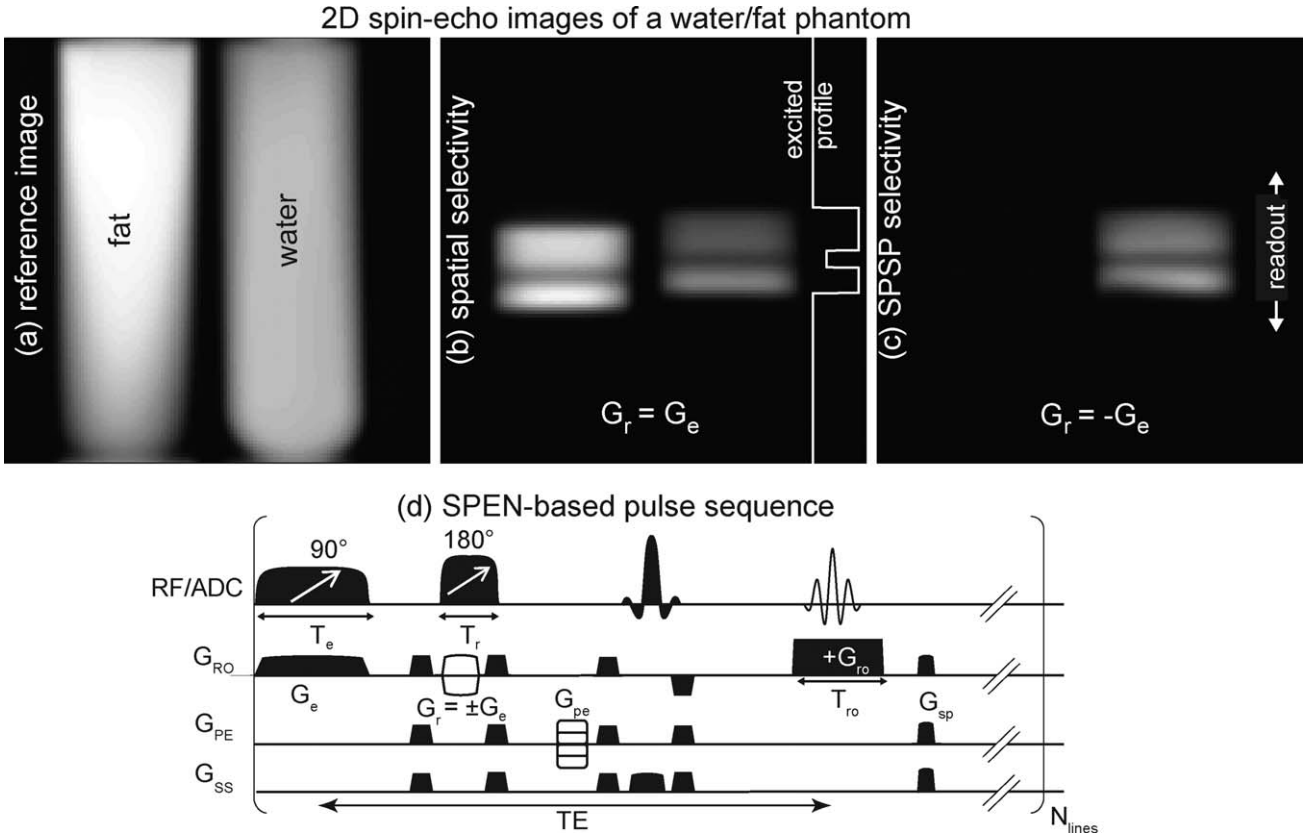

FIG. 3. **a**: Reference image of examined water/fat phantom with no spectral or in-slice spatial selectivity. **b**,**c**: Spin-echo images illustrating the spatial and spectral selectivity achievable by SPEN, obtained with the sequence shown in (**d**). Part (b) utilizes $G_e = G_r$ whereas (c) utilizes $G_e = -G_r$ as gradients for excitation and refocusing. The excitation pulse is obtained using the small-tip-angle approximation for a non-uniform shape of $L = 5$ mm width. Pulses have a bandwidth of 10.5 kHz and a duration $T_e = 16$ ms and $T_r = 8$ ms. The frequency sweeps have a duration $T'_e = 10$ ms for excitation and $T'_e/2$ for refocusing. The echo time (TE) and repetition time (TR) are TE/TR = 38/5000 ms. 128 × 64 points are acquired for a field of view of 2.5 × 2.5 cm^2; 100 × 64 points centered around the water echo are filtered, zero filled to 128 × 128, apodized with a Hamming window and Fourier transformed.

pulses were applied along the slice-selection dimension in simultaneity with the phase-encoding blips of the EPI gradient waveform. Separate Fourier transformation of the odd and even EPI echoes thus yielded separated water and fat images, from a common slice-selected region.

All pulses were generated and all images were processed offline using suitable Matlab® scripts (The Mathworks, Natick, MA), available upon request. Pulses were designed and clocked out with 4 μs time-steps; additional details are given in the corresponding figure captions.

RESULTS

Spectral-Spatial Selectivity: 7 T Phantom Tests and Results

Experiments were first implemented to confirm the spatial and spectral selectivities of the SPEN-based approach, using the simple water/fat phantom shown in Figure 3a. For better assessing the spatial-selecting abilities, 90°/180° frequency-swept pulses were applied in these tests along the readout axis—even if under normal use one would apply these SPEN-based pulses along the slice-selection dimension. Figure 3b shows the profile obtained upon using a sequence devoid from chemical-shift selectivity, which employs equal-gradient and equal-signed sweeps for excitation and refocusing. This panel also illustrates the possibility to obtain a non-uniform intensity. The possibility to integrate a shift-selectivity into this scheme is illustrated in Figure 3c. In this case the pair of frequency-swept pulses was applied as shown in Figure 1, with $G_e = -G_r$. The ensuing shift-dependent spatial winding (Eq. [2]) results in the expected k_{cs}-shifts of the water and fat echoes. A water-only image can thus be obtained, by timing the readout echoing gradients so as to refocus solely this resonance while keeping the fat dephased.

These pulses can provide a practical means to achieve chemical-shift specificity together with slice selectivity. This is further illustrated in Figure 4. Whereas the $G_e = G_r$ conditions in panel (a) lead to no shift selectivity, the residual fat signal remaining upon selectively choosing the water chemical shift focus (panel b) is less than 2% of its original value. Moreover, as fat is coherently

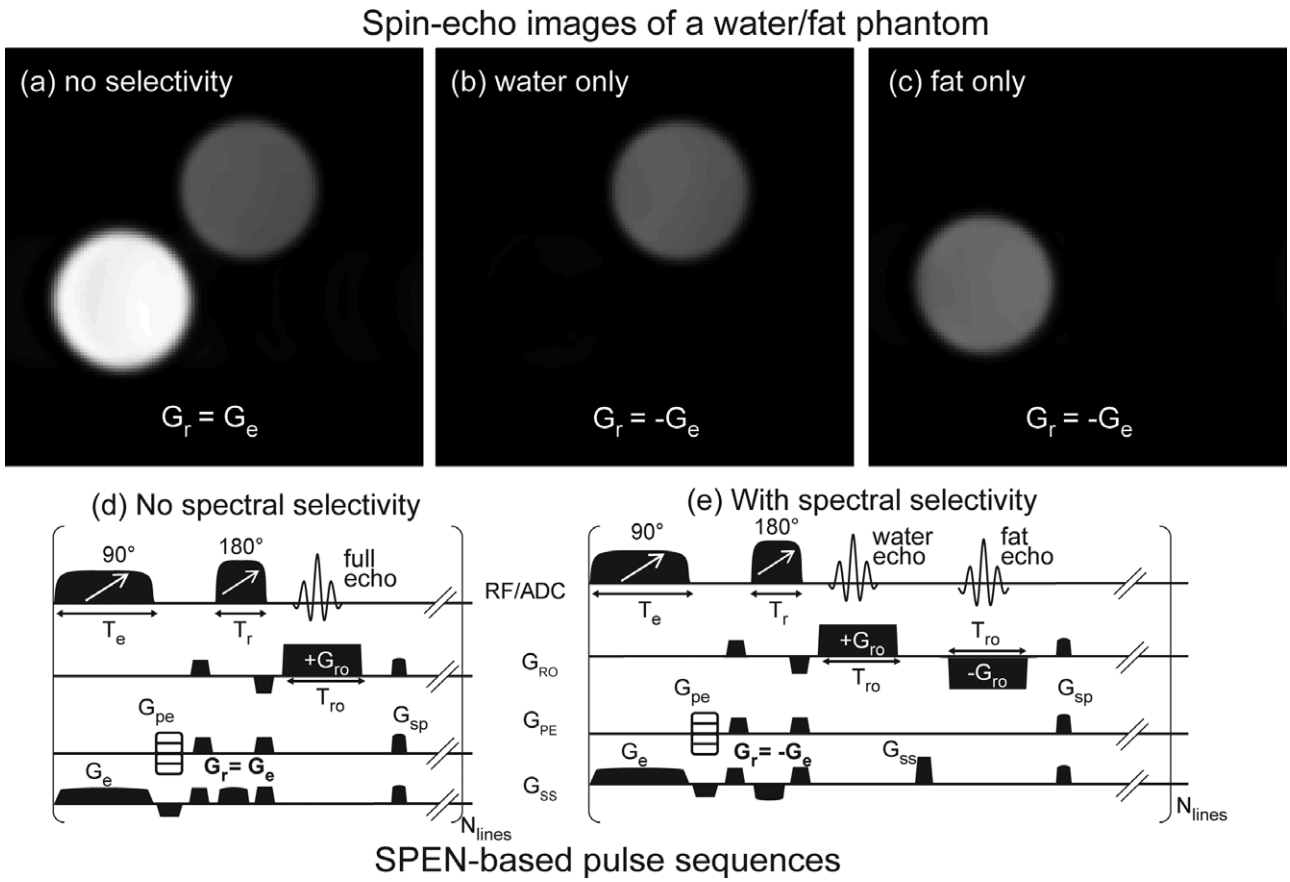

FIG. 4. Slice-selective spin-echo imaging of the water/fat phantom introduced in Figure 3a. **a**: Simultaneous water/fat echoes formed upon using the sequence shown in (**d**), with $G_e = G_r$ and quadratic-phase SLR 90/180° pulses. **b**,**c**: Separated, concurrent water and fat images collected using the sequence in (**e**), incorporating $G_r = -G_e$ and a fat echo forming 2 ms after the water echo by playing a gradient lobe in the slice-selection dimension and reversing the readout gradient. The SLR pulses have a bandwidth of 10.5 kHz and a duration $T_e = 4.8$ ms for excitation and $T_r = 3.2$ ms for refocusing, and the sweep durations are $T'_e = 3.0$ ms for excitation and $T'_e/2$ for refocusing. The slice thickness is $L = 5$ mm in all panels and 64 × 64 points are acquired with a field of view of 2.5 × 2.5 cm^2 and TE(water)/TE(fat)/TR = 14/16/1000 ms. The data is zero-filled to 128 × 128 and apodized with a Hamming window before Fourier transformation.

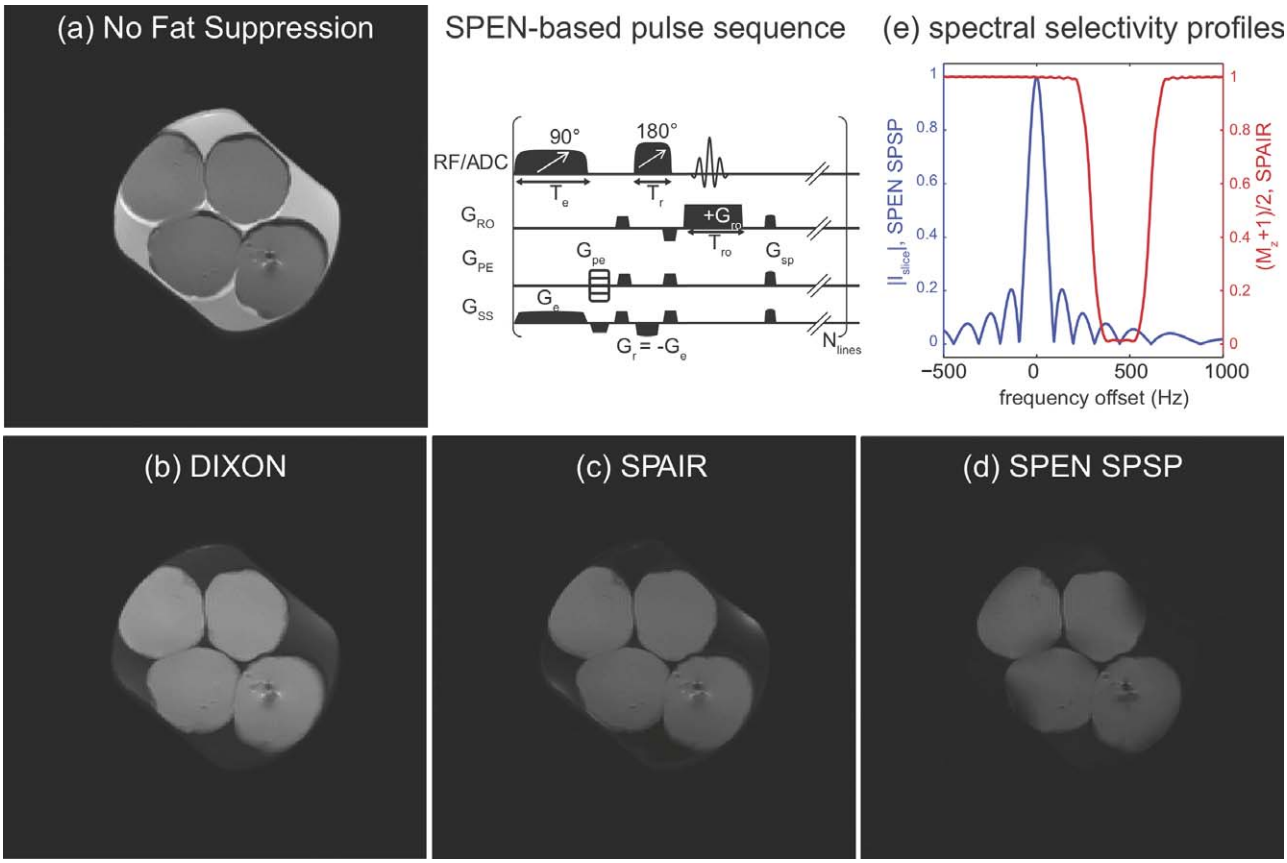

FIG. 5. Slice-selective spin-echo imaging of a water/fat phantom consisting of four water-containing spheres immersed in oil. A comparison is made between a reference image without fat suppression (**a**), and fat-suppressed sequences based on the Dixon (**b**), the SPAIR (**c**), and our new SPEN-based SPSP (**d**) sequences. The slice thickness is $L = 6$ mm and 256 × 205 points are acquired with a field of view of 18 × 18 cm^2. TE/TR = 24/1000 ms. For the extended two-point Dixon method, the echo time is TE = 49.2 ms for the second echo, which is acquired in the same shot after a refocusing pulse. The SPEN-based sequence, shown as an inset, relied on SLR pulses with 4.5 kHz bandwidths, a $T_e = 9.6$ ms duration for excitation and $T_r = 6$ ms for refocusing, and sweep durations $T'_e = 5.6$ ms for excitation and $T'_e/2$ for refocusing. **e**: Comparisons between the spectral selectivities of the SPEN-SPSP and the SPAIR pulse sequences. [Color figure can be viewed in the online issue, which is available at wileyonlinelibrary.com.]

dephased within the well-defined excited slice, a suitable k_{cs} gradient lobe in the slice-selection dimension can be used to rephase it while simultaneously dephasing the water. A fat echo can thus be acquired immediately following the acquisition of the water echo, as shown in Figure 4c. The drop in the latter's signal intensity compared to a standard slice-selective spin-echo excitation is 50%, and can be explained by the reduced slice thickness associated to the off-resonant effects, plus a small T_2^* weighting related to the 2 ms delay between the water and the fat echoes in the concurrent acquisition.

Spectral-Spatial Selectivity: 3 T Phantom Tests and Results

Further insight into the mechanism and performance of the SPEN SPSP approach can be obtained by comparing its images against alternatives obtained with canonical fat-suppression sequences. Figure 5 shows such comparisons for two well-established techniques, SPAIR and the extended two-point Dixon method, together with a non-fat-suppressed image. The distinct consequences of field inhomogeneities can be readily appreciated in this figure: the Dixon-based method is least sensitive to inhomogeneities but less spectrally selective; the different performance between SPAIR and SPEN SPSP arises from the spectral selectivity profile shown in Figure 5e, which illustrates how the former achieves a selective fat suppression while the latter achieves a selective water excitation. It should also be noted that, among all these techniques, only the SPEN-based SPSP approach simultaneously provides spectral selectivity and spatial localization.

Spectral-Spatial Selectivity: 3 T Human Volunteer Studies

To explore the pulses' ability to deal with the challenges arising in vivo, the method was assayed at 3 T with a series of breast imaging scans on female volunteers. Selectivity is then complicated by the smaller chemical-shift difference between the sites (≈450 Hz), as well as by the higher heterogeneities characterizing these experiments. Figure 6 compares both sagittal and axial imaging results arising from two different multi-scan sequences: spin-echo images collected using scanner-supplied

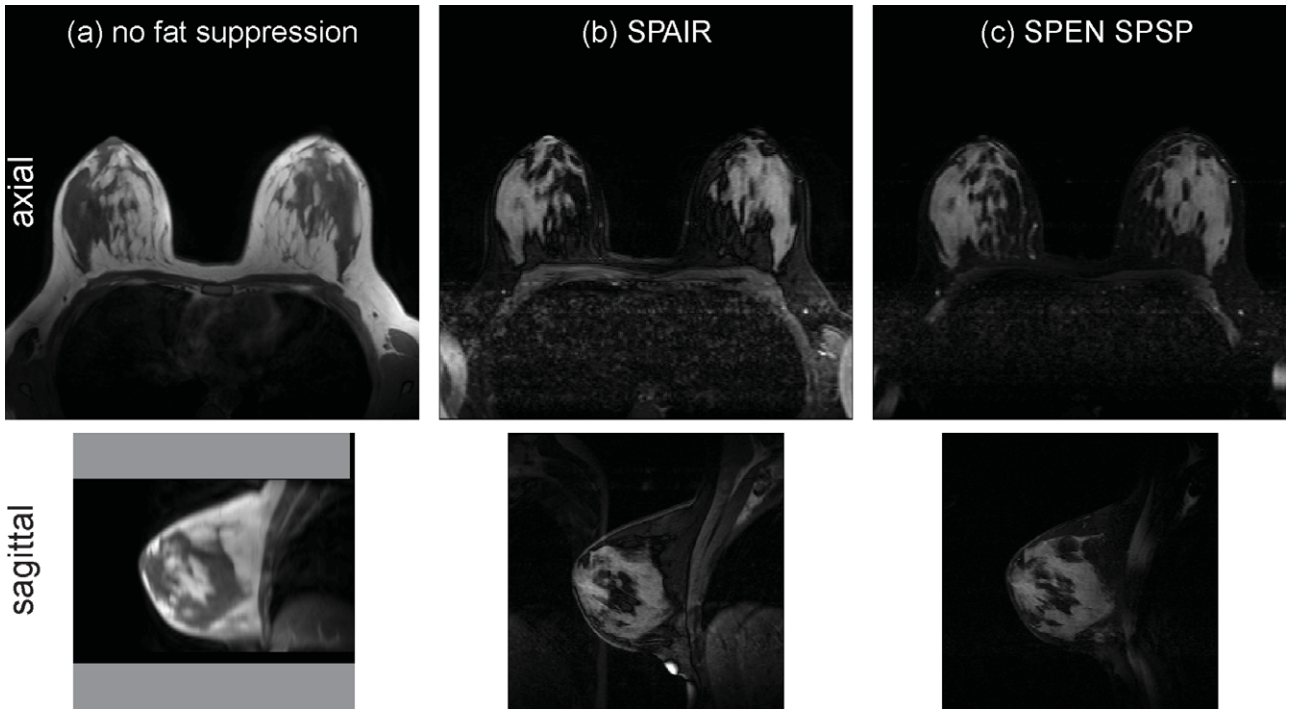

FIG. 6. Multi-shot spin-echo imaging of human breast at 3 T. A comparison is made between a reference image (**a**), and both SPAIR-based (**b**) and a SPEN-based SPSP (**c**) sequences incorporating fat suppression. The slice thickness in (b) and (c) is $L = 5.5$ mm and 256×128 points are acquired with a field of view of 33×33 cm^2 for axial images and 24×24 cm^2 for sagittal images. TE/TR = 24/400 ms. For the SPEN-based SPSP selectivity, the pulses are as described in Figure 5. The reference images with no fat suppression are obtained by volume rendering from an axial, multi-slice, T_1-weighted gradient-echo image. The slice thickness is 2.5 mm and 448×448 points are acquired with a field of view of $36 \times 36 \times 15$ cm^3; TE/TR = 2.5/6.8 ms, flip angle = 18°, and areas outside the acquired volume are shown in gray. Power deposition for five slices, as calculated by the scanner-supplied software, is 11% for the SPAIR sequence and 34% for the SPEN SPSP sequence.

SPAIR pulses, and spin-echo images arising upon performing SPEN-based SPSP pulses refocusing the water but not the fat resonances. A conventional gradient-echo image is also shown in (a) to illustrate the water/fat contrast according to the natural T_1 differences related to the anatomy of connective and fatty tissues. In this example, where identical acquisition parameters are employed for the two fat-suppression techniques, a cleaner separation of the connective tissues can be appreciated in the SPEN SPSP experiments; also sharper features are revealed upon using the SPSP pulses. A thorough comparison will be required to assess the relative merits of these methods in application-specific studies but this illustrative example validates the idea of using SPEN for spectral-spatial selectivity.

One of the main uses of 2D spectral-spatial selectivity centers on EPI acquisitions of multi-slice 2D water images. Given its relatively low bandwidth in the phase encoding direction, this single-shot technique usually requires an efficient suppression of fat signals that would otherwise lead to significantly shifted or blurred contributions. Figure 7a illustrates how the SPEN-based SPSP selectivity can be used for fat suppression in multi-slice spin-echo EPI. EPI, a basic tool in several applications such as diffusion-weighted MRI (36,37), is a method that given its single-scan, low-bandwidth nature requires good fat suppression (38,39). This is particularly true for breast imaging, which can provide qualitative and quantitative information about tissue and lesion types (40,41). When this kind of experiment was examined (Fig. 7a and b), the level of fat suppression observed using the SPEN-bases SPSP pulses was comparable—and in fact somewhat higher—than that achieved with selective water excitation using the scanner-supplied 2D SPSP pulses. Figure 7c illustrates another opportunity opened by the SPEN scheme, this time focused on the simultaneous acquisition of water and fat images in a single shot. In this approach, the two species are imaged simultaneously with water contributing only to the odd echoes and fat contributing to the even ones. A choice was made to halve the field of view along the phase-encoded dimension; other options, such as halving the resolution or doubling the acquisition time, are also possible.

DISCUSSION

Pairs of frequency-swept pulses have been used in the past for spatial localization within an MRI context (8,10,23–25); frequency-swept manipulations under the action of gradients are also an integral component of ultrafast 2D MRS spectral characterizations. In the present study, we investigated the use of these manipulations in a hybrid setting, aiming to achieve both spatial

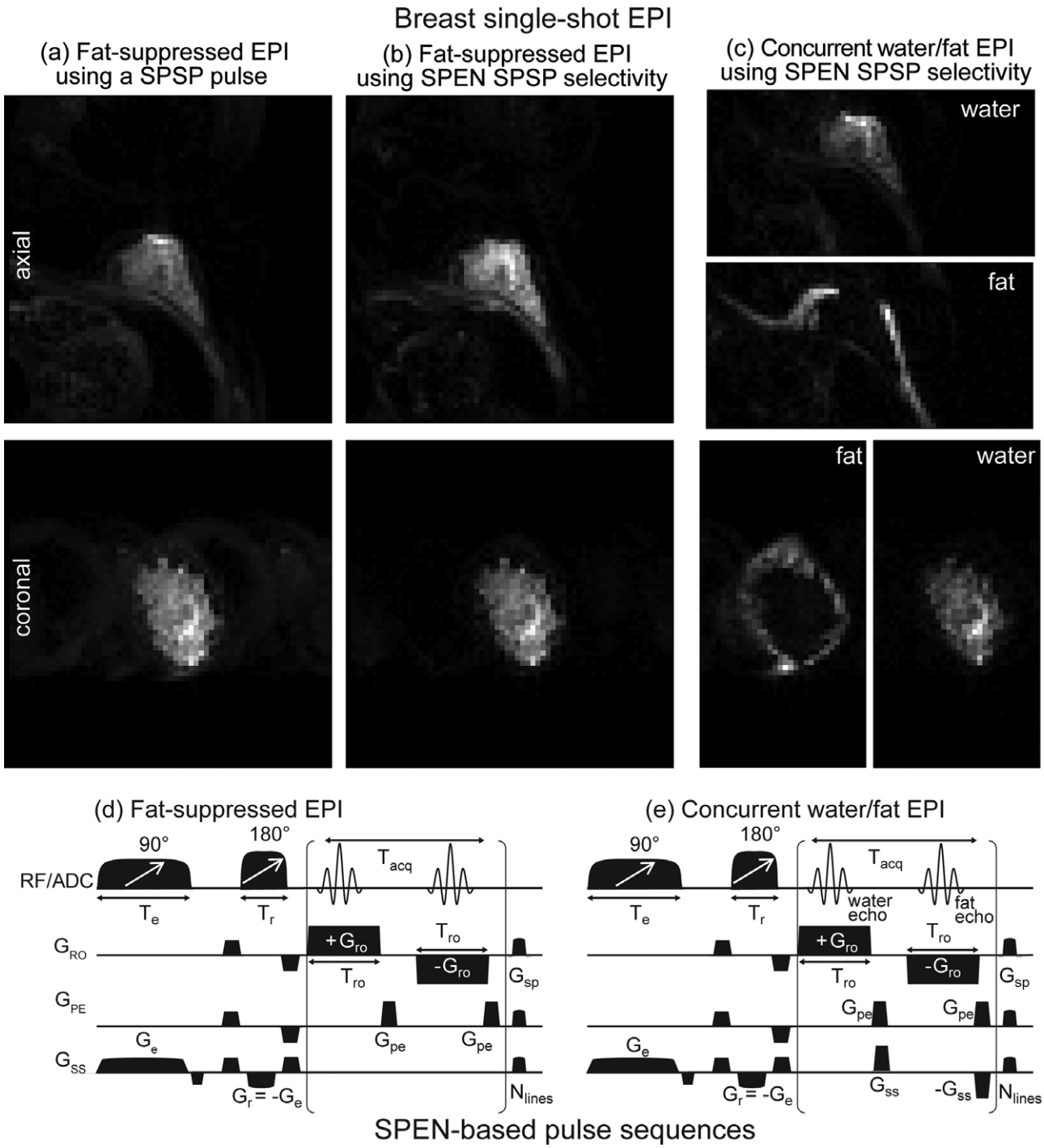

FIG. 7. Breast spin-echo EPI images collected at 3 T using: (**a**) a scanner-supplied SPSP 2D pulse for slice-selective water excitation; (**b**) the SPEN-based SPSP selectivity (sequence shown in (**d**)). The slice thickness is $L = 5$ mm and 64 $\times$ 64 points are acquired with a field of view of 22 $\times$ 22 cm^2 and TE = 44 ms. Images are obtained in a single-shot ($N_{lines} = 64$) with the minimum echo time achievable with the SPEN-based pulses. **c**: Concurrent single-shot spin-echo EPI water and fat images collected using the SPEN-based SPSP sequence shown in (**e**). The slice thickness is 10 mm and 64 $\times$ 32 points are acquired for each species with a field of view of 22 $\times$ 11 cm^2 and TE = 72 ms. For the SPEN-based SPSP selectivity, the pulses are as described in Figure 5.

and spectral selectivity. This represents another use of SPEN-based concepts for achieving a selective 2D patterning, of the kind that has been recently demonstrated in a purely spatial-spatial setting (42). By contrast to such earlier study, however, this study focuses on providing an additional degree of spectral selectivity. When compared to conventional 2D spectral-spatial pulses (3,4), the most evident feature of the SPEN-based SPSP selectivity is its avoidance of oscillating gradient waveforms. The demands on gradient hardware and

timing accuracy are thus relaxed; in addition better slice profiling (and in general, improved spatial sculpting) opportunities are opened by the SPEN-based pulses, which rely on much longer irradiation periods for imparting their spatial manipulations.

Despite these advantages, certain limitations are evident in the SPEN SPSP procedure. Foremost among these is the fact that all species in the sample will be excited by the 90°/180° combination here described with the same flip angle; an undesirable situation, particularly in ultrafast spectroscopic imaging studies of hyperpolarized metabolites. Another limitation is their sensitivity to field inhomogeneities, which can lead to losses in the water signal as well as to contaminations by the fat signal, particularly at lower field strengths. Other offset-based methods such as SPAIR and conventional SPSP pulses share this limitation, while Dixon-based methods can show improved robustness against B_0 inhomogeneity. An additional mechanism that could influence the specific performance of frequency-swept SPSP pulses—including their effective SNR and contrast—concerns spin relaxation during the frequency-swept pulses, particularly transverse rotating frame relaxation ($T_{2\rho}$) over the course of the 90° excitation and 180° inversion. An additional diffusion weighting could arise, given the gradients and non-linear-phases introduced during the course of the pulse (43). Neither of these effects was detrimental in the present study given the short durations of the frequency sweeps used, but they should be kept in mind when designing experiments that rely on longer SPEN manipulations.

CONCLUSIONS

SPEN concepts were used to design a simple way of achieving simultaneous spatial and spectral selectivity. In contrast to traditional 2D SPSP pulses, this SPEN-based selectivity does not require fast oscillating gradients and can impart a high-definition spatial profile without compromising on the spectral selectivity. The approach was shown useful for fat suppression in both multi-shot and single-shot spin-echo imaging. In both cases it was shown how a simple modification can lead to the concurrent collection of water and fat images; extensions to additional species can be readily devised, suggesting the possible use of such schemes for the fast spectroscopic imaging of hyperpolarized metabolites.

ACKNOWLEDGMENTS

Authors thank Prof. H. Degani, Dr. E. Furman-Haran and the MRI technician team (Weizmann Institute) as well as Dr. S. Shushan (Wolfson Medical Center) for assistance with the human imaging.

REFERENCES

1. Bernstein MA, King KF, Zhou XJ. Handbook of MRI pulse sequences. New York: Academic Press; 2004.
2. de Graaf RA. In vivo NMR spectroscopy. Chichester: Wiley; 2007.
3. Meyer CH, Pauly JM, Macovski A, Nishimura DG. Simultaneous spatial and spectral selective excitation. Magn Reson Med 1990;15:287–304.
4. Zur Y. Design of improved spectral-spatial pulses for routine clinical use. Magn Reson Med 2000;43:410–420.
5. Lau AZ, Chen AP, Hurd RE, Cunningham CH. Spectral-spatial excitation for rapid imaging of DNP compounds. NMR Biomed 2011;24:988–996.
6. Pauly J, Nishimura D, Macovski A. A k-space analysis of small-tip-angle excitation. J Magn Reson 1989;81:43–56.
7. Freeman R. Spin choreography. Oxford: Oxford University Press; 1998.
8. Garwood M, DelaBarre L. The return of the frequency sweep: designing adiabatic pulses for contemporary NMR. J Magn Reson 2001;153:155–177.
9. Bohlen JM, Rey M, Bodenhausen G. Refocusing with chirped pulses for broad-band excitation without phase dispersion. J Magn Reson 1989;84:191–197.
10. Conolly S, Glover G, Nishimura D, Macovski A. A reduced power selective adiabatic spin-echo pulse sequence. Magn Reson Med 1991;18:28–38.
11. Kunz D. Use of frequency-modulated radiofrequency pulses in MR imaging experiments. Magn Reson Med 1986;3:377–384.
12. Tal A, Frydman L. Single-scan multidimensional magnetic resonance. Prog Nucl Magn Reson Spectrosc 2010;57:241–292.
13. Ben-Eliezer N, Shrot Y, Frydman L. High-definition, single-scan 2D MRI in inhomogeneous fields using spatial encoding methods. Magn Reson Imaging 2010;28:77–86.
14. Shrot Y, Frydman L. Spatially encoded NMR and the acquisition of 2D magnetic resonance images within a single scan. J Magn Reson 2005;172:179–190.
15. Tal A, Frydman L. Spatial encoding and the single-scan acquisition of high definition MR images in inhomogeneous fields. J Magn Reson 2006;182:179–194.
16. Chamberlain R, Park J-Y, Corum C, Yacoub E, Ugurbil K, Jack CR Jr, Garwood M. Raser: a new ultrafast magnetic resonance imaging method. Magn Reson Med 2007;58:794–799.
17. Frydman L, Scherf T, Lupulescu A. The acquisition of multidimensional NMR spectra within a single scan. Proc Natl Acad Sci USA 2002;99:15858–15862.
18. Mishkovsky M, Frydman L. Principles and progress in ultrafast multidimensional nuclear magnetic resonance. Annu Rev Phys Chem 2009;60:429–448.
19. Gal M, Frydman L. Ultrafast multidimensional NMR: principles and practice of single-scan methods. Encyclopedia of magnetic resonance. eMagRes 2008. doi: 10.1002/9780470034590.emrstm1024.
20. Shrot Y, Frydman L. Spatial encoding strategies for ultrafast multidimensional nuclear magnetic resonance. J Chem Phys 2008;128:052209.
21. Pelupessy P. Adiabatic single scan two-dimensional NMR spectroscopy. J Am Chem Soc 2003;125:12345–12350.
22. Pipe JG. Spatial encoding and reconstruction in MRI with quadratic phase profiles. Magn Reson Med 1995;33:24–33.
23. Balchandani P, Khalighi MM, Glover G, Pauly J, Spielman D. Self-refocused adiabatic pulse for spin echo imaging at 7 T. Magn Reson Med 2012;67:1077–1085.
24. Kunz D. Frequency-modulated radiofrequency pulses in spin-echo and stimulated-echo experiments. Magn Reson Med 1987;4:129–136.
25. Park J-Y, Garwood M. Spin-echo MRI using pi/2 and pi hyperbolic secant pulses. Magn Reson Med 2009;61:175–187.
26. Shrot Y, Shapira B, Frydman L. Ultrafast 2D NMR spectroscopy using a continuous spatial encoding of the spin interactions. J Magn Reson 2004;171:163–170.
27. Andersen NS, Kockenberger W. A simple approach for phase-modulated single-scan 2D NMR spectroscopy. Magn Reson Chem 2005;43:795–797.
28. Tal A, Shapira B, Frydman L. A continuous phase-modulated approach to spatial encoding in ultrafast 2D NMR spectroscopy. J Magn Reson 2005;176:107–114.
29. Pauly J, Leroux P, Nishimura D, Macovski A. Parameter relations for the Shinnar-Le Roux selective excitation pulse design algorithm. IEEE Trans Med Imaging 1991;10:53–65.
30. Balchandani P, Pauly J, Spielman D. Designing adiabatic radio frequency pulses using the Shinnar-Le Roux algorithm. Magn Reson Med 2010;64:843–851.
31. Schulte RF, Tsao J, Boesiger P, Pruessmann KP. Equi-ripple design of quadratic-phase rf pulses. J Magn Reson 2004;166:111–122.

32. Shinnar M. Reduced power selective excitation radio-frequency pulses. Magn Reson Med 1994;32:658–660.
33. Lauenstein TC, Sharma P, Hughes T, Heberlein K, Tudorascu D, Martin DR. Evaluation of optimized inversion-recovery fat-suppression techniques for T2-weighted abdominal MR imaging. J Magn Reson Imaging 2008;27:1448–1454.
34. Dixon WT. Simple proton spectroscopic imaging. Radiology 1984;153:189–194.
35. Skinner TE, Glover GH. An extended two-point dixon algorithm for calculating separate water, fat, and B-0 images. Magn Reson Med 1997;37:628–630.
36. Basser PJ. Inferring microstructural features and the physiological state of tissues from diffusion-weighted images. NMR Biomed 1995;8:333–344.
37. Turner R, Lebihan D, Chesnick AS. Echo-planar imaging of diffusion and perfusion. Magn Reson Med 1991;19:247–253.
38. Block W, Pauly J, Kerr A, Nishimura D. Consistent fat suppression with compensated spectral-spatial pulses. Magn Reson Med 1997;38:198–206.
39. Schmitt F, Stehling MK, Turner R, Mansfield P. Echo-planar imaging: theory, technique and application. Berlin: Springer; 1998.
40. Paran Y, Bendel P, Margalit R, Degani H. Water diffusion in the different microenvironments of breast cancer. NMR Biomed 2004;17:170–180.
41. Woodhams R, Ramadan S, Stanwell P, Sakamoto S, Hata H, Ozaki M, Kan S, Inoue Y. Diffusion-weighted imaging of the breast: principles and clinical applications. Radiographics 2011;31:1059–1084.
42. Dumez JN, Frydman L. Multidimensional excitation pulses based on spatiotemporal encoding concepts. J Magn Reson 2013;226:22.
43. Shrot Y, Frydman L. The effects of molecular diffusion in ultrafast two-dimensional nuclear magnetic resonance. J Chem Phys 2008;128:164513.